# *Ab initio* investigation of structural stability and exfoliation energies in transition metal dichalcogenides based on Ti-, V-, and Mo-group elements

Carlos M. O. Bastos,[1] Rafael Besse,[1] Juarez L. F. Da Silva,[2] and Guilherme M. Sipahi[1,*]
[1]*São Carlos Institute of Physics, University of São Paulo, P.O. Box 369, 13560-970 São Carlos, SP, Brazil*
[2]*São Carlos Institute of Chemistry, University of São Paulo, P.O. Box 780, 13560-970 São Carlos, SP, Brazil*

(Received 5 October 2018; revised manuscript received 30 January 2019; published 10 April 2019)

In this work, we report an *ab initio* investigation based on density functional theory of the structural, energetic, and electronic properties of 2D layered chalcogenides compounds based in the combination of the transition-metals (Ti, Zr, Hf, V, Nb, Ta, Cr, Mo, W) and chalcogenides (S, Se, Te) in three polymorphic phases: trigonal prismatic (2H), octahedral (1T), and distorted octahedral ($1T_d$). We determined the most stable phases for each compound, verifying the existence of the $1T_d$ phase for a small number of the compounds and we have also identified the magnetic compounds. In addition, with the determination of the exfoliation energies, we indicated the potential candidates to form one layer material and we have also found a relation between the exfoliation energy and the effective Bader charge in the metal, suggesting that when the materials present small exfoliation energies, it is due to the Coulomb repulsion between the chalcogen planes. Finally, we analyzed the electronic properties, identifying the semiconductor, semimetal, and metal materials and predicting the band gap of the semiconductors. In our results, the dependence of the band gap on the *d*-orbital is explicit. In conclusion, we have investigated the properties of stable and metastable phases for a large set of TMD materials, and our findings may be auxiliary in the synthesis of metastable phases and in the development of new TMDs applications.

DOI: 10.1103/PhysRevMaterials.3.044002

## I. INTRODUCTION

Layered materials have been known for 50 years [1] and are applied in areas as diverse as dry lubricants [2], batteries [3], catalysts [4], among others. Recently, layered transition-metal dichalcogenides (TMDs), materials with chemical formula $MQ_2$, with $M$ being a transition-metal and $Q$ a chalcogen (S, Se, and Te), have attracted wide technological interest due to their capacity of being isolated into one layer, like graphene does [5,6], and the wide spectrum of the electronic properties they present, being metals, semimetals, semiconductors, and insulators [7]. Recently, there were reported TMDs presenting exotic electronic properties, such as having topological insulator states [8], being a Weyl semimetal [9], and displaying charge density waves [7]. The wide spectrum of properties presented by TMDs is enabled by their large number of chemical compositions combining $M$ and $Q$ and the existence of several polymorphic phases [5,7,10].

In TMDs, layers composed of covalently bound $M$ and $Q$ planes are bound to each other by van der Waals interactions, and distinct coordination environments of the metal atoms within each layer generate structural polymorphism in these materials. Among these polymorphic phases, we highlight the most stable ones for a wide variety of materials [10,11]: (i) trigonal prismatic (2H), (ii) octahedral (1T), and (iii) distorted octahedral ($1T_d$). The lowest energy polymorph for a TMD depends mainly on the atomic radii and on the filling of the metal *d*-orbitals [11], e.g., Ti group metals (Ti, Zr, and Hf) favor 1T as the lowest energy phase [12]. However, the Peierls distortion mechanism is crucial for the energetic favoring of the $1T_d$ phase in some compounds, since it breaks the degeneracy of electronic states, reducing the energy [12,13].

The coexistence among different phases is linked to parameters such as temperature or pressure [14,15], and for the same material two different polymorphic phases may drastically change properties, e.g., $MoS_2$ in 2H and 1T phase is a semiconductor and a metal, respectively [16,17]. The synthesis of many polymorphic phases has been possible with the advance of experimental techniques [18–21], allowed to obtain polymorphic phases which are not at the lowest energies. However, few studies were done in these metastable phases and a comprehensive characterization of TMD compounds and polymorphs is important to explore their properties and identify stability factors.

A key factor for the renewed interest in layered TMDs is the production of two-dimensional (2D) materials from the mechanical or chemical exfoliation of the layers [22]. The easiness to exfoliate the materials comes from the weak binding between layers, which depends on the van der Waals interactions, much weaker than the in-plane covalent bonding. However, some materials are more difficult to exfoliate than others due to stronger interlayer binding and, as suggested by Monet *et al.* [23], the exfoliation energy can be used to determine how easy it is to exfoliate the layers from the crystal. Previous studies report exfoliation energies only for TMDs at the lowest energy phases and studies involving another polymorphic phases are not common. Therefore, a thorough evaluation of the exfoliation energy in different TMD compounds and polymorphs is called for as an effective way to guide the production of two-dimensional materials.

To obtain a comprehensive description of the properties of layered TMDs, we performed a first-principles investigation of the stability, exfoliation energy, and electronic properties

*Corresponding author: sipahi@ifsc.usp.br

 

of TMDs formed by Ti-, V-, and Cr-group transition metals and S, Se, and Te, in three different polymorphic phases: 2H, 1T, 1T′. The elastic constants of the materials were calculated, which provide means to evaluate their stability, and the magnetic order was also considered. Based on the exfoliation energies and on the analysis of charge transfer between metals and chalcogens, we identified trends correlating the intralayer charge transfer with the magnitude of interlayer binding. Last, we classified all the studied TMDs compositions and polymorphic phases according to their electronic properties.

## II. THEORETICAL APPROACH AND COMPUTATIONAL DETAILS

Our first-principles calculations are based on the density functional theory (DFT) formalism [24,25] within the semilocal exchange and correlation functional proposed by Perdew–Burke–Ernzerhof (PBE) [26]. The Kohn–Sham equations were solved using the PAW method [27] as implemented in the Vienna *ab initio* simulation package (VASP), version 5.4.1 [28,29]. We focus on layered dichalcogenides, and it is well known from the literature that the PBE functional underestimates long-range interactions such as the London dispersion [30]. To minimize this problem, we employed the semiempirical DFT-D3 method proposed by Grimme *et al.* [31], which has been shown to provide structural properties for $MoS_2$ in good agreement with experimental results [32].

It has been well known that (semi-)local functionals fail to accurately predict band gap energies [33–38], and hence, to minimize this problem, the electronic properties, such as density of states (DOS) and band structures, were computed using the hybrid functional proposed by Heyd–Scuseria–Ernzerhof [39,40] (HSE06), which contains the PBE correlation and separates the exchange term in long- and short-range terms by a screening function with the parameter $\omega = 0.206\,\text{Å}^{-1}$. The short-range term is composed of 25% of exact exchange and 75% of PBE exchange, while the long-range term is composed only by PBE exchange. We included also the relativistic effects of spin-orbit-coupling (SOC) for the valence states through the second-variational approach [41].

Spin-orbit coupling (SOC) effects were included for the valence states through the second-variational approach [41]. As showed in our previous work [38], the SOC have small impact in the structural properties, hence, for volume equilibrium, relative energy stability, exfoliation energy, and elastic constants calculations, the SOC was neglected. For electronic properties, such as band structures and DOS, SOC corrections were considered only in combination with the PBE functional, due to the high computational cost of the combined HSE06-SOC calculations.

Structural optimizations were performed with PBE+D3 through the minimization of the stress tensor and of the forces on every atom. We used, for the plane-waves basis set, cutoff energy of 2× the maximum energy recommended by VASP (ENMAX parameter from POTCAR file, as described in Table I of the Supplemental Material [42]) to determine the equilibrium lattice parameters. Using the optimized structures, the elastic constants were computed using (i) contributions from strain-stress relations for distortions in the lattice with rigid ions and (ii) ionic relaxation contributions, determined from the inversion of ionic Hessian matrix [43,44]. To achieve the convergence condition for the elastic constant we increased the cutoff energy to 2.5×ENMAX. The cutoff energy employed to compute the electronic properties, i.e., DOS, band structure, and Bader charge, as well as to obtain cohesive energy and exfoliation energy, was 1.125×ENMAX.

For the integration in the first Brillouin zone, we employed a Monkhorst–Pack scheme [45] using a **k**-mesh of 11×11×2 for 2H-$MoS_2$, and meshes with same **k**-point density for the remaining structures, to obtain the equilibrium structure parameters. However, the **k**-mesh was increased in all systems, e.g., to 22×22×5 for 2H-$MoS_2$, to compute the electronic properties. Due to the limitations of parallel calculations of elastic constants in VASP, we employed a Γ-centered **k**-mesh with fixed grid of 16×16×4, 12×12×6, and 10×18×5 for 2H, 1T, and $1T_d$ structures, respectively, for all chemical compositions. More details about the computational approach are provided in the Supplemental Material [42].

## III. CRYSTAL STRUCTURES: $MQ_2$

Our study concentrates on the most commonly observed TMD structural phases, 2H, 1T, and $1T_d$ [7]. In Fig. 1, we present the schematics of the polytypes crystal structures, with Figs. 1(a)–1(c) showing the top and lateral views and Fig. 1(d) indicating an example of supercell employed to access the magnetic ordering. The 2H structure, shown in Fig. 1(a), is composed of a hexagonal lattice, with 2 formula units (f.u.) per unit cell, whose atoms planes are in the AbA BaB stacking sequence (capital and lower case letters for chalcogen and metal atoms planes, respectively), belonging to the $P6_3/mmc$ space group [10]. The 1T structure, shown in Fig. 1(b), is composed of a hexagonal lattice with 1 f.u. per unit cell, with AbC AbC stacking sequence, belonging to the $P\bar{3}m1$ space group [10]. Each layer of the $1T_d$ structure, shown in Fig. 1(c), can be generated from a 1T monolayer by reconstructions in a 2×1 orthorhombic cell, originating dimerized lines of metal atoms, a distortion which has been shown to be driven by a Peierls transition mechanism [13]. The $1T_d$ structure is composed of an orthorhombic lattice with 4 f.u. in the unit cell, belonging to the $Pnm2_1$ space group. The bonding geometry symmetries correspond to $D_{6h}$, $D_{3d}$, and $C_{2v}$ point groups for 2H, 1T, and $1T_d$, respectively.

We address materials composed by Ti-, V-, and Mo-group metals, with not fully occupied $d$-orbitals, thus some of the TMDs can exhibit nonzero magnetic moment, as has been experimentally observed in $VS_2$ and $VSe_2$ with ferromagnetic ordering in low temperatures [10,46]. To address the intrinsic magnetism in bulk TMDs, we employed supercells containing eight f.u., allowing to model antiferromagnetic configurations, as exemplified in Fig. 1(d). For nonmagnetic and ferromagnetic orderings, the unit cell was employed, since it can represent such configurations. To increase the reliability of our results, we built four antiferromagnetic initial configurations with supercells, plus the ferromagnetic one, and equilibrium volumes were obtained for every initial configuration, from which the lowest energy structure was subsequently selected. Tables with the energy comparison for the five initial configurations can be found in the Supplemental Material [42].

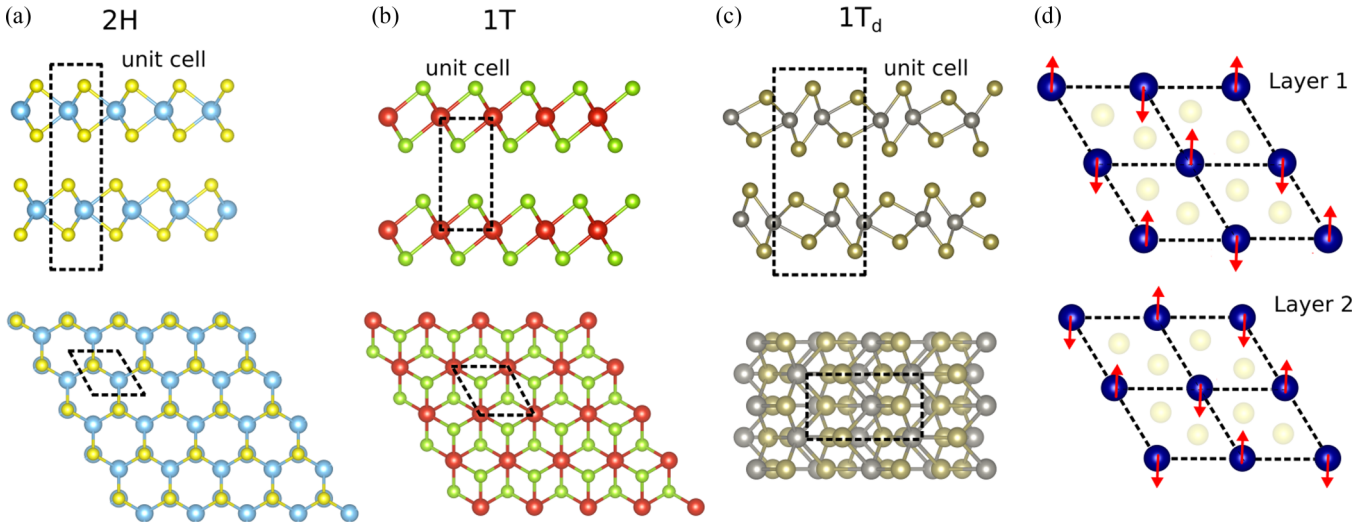


FIG. 1. Lateral and top view of the TMDs crystal structures of polytypes (a) trigonal prismatic (2H), (b) octahedral (1T), and (c) distorted octahedral (1T$_d$). The unit cells are represented in dashed lines. (d) Example of the supercell used to obtain the magnetic ordering, where the red arrows represent the initial magnetic moments in transition metal atoms.

## IV. RESULTS

### A. Relative energy stability

We obtained the equilibrium geometric configurations for all compounds and analyzed the relative stability between the phases (2H, 1T, 1T$_d$) by comparison of the total energy, Fig. 2. For Ti group compounds, V group selenides and tellurides, and $CrTe_2$, the 1T$_d$ phase does not present a local minimum structure in the potential surface, i.e., even if the structural relaxation starts from the 1T$_d$ structure, it yields the structural configuration of the 1T phase. Therefore, these compounds are not stable in the 1T$_d$ phase and these structures were not further considered in our calculations.

Figure 2 shows the relative total energies obtained for the three polymorphic phases using 2H phase as the reference. For all the Ti group compounds (Ti, Zr, and Hf combined with S, Se, and Te) the lowest energy phase is 1T, as expected [5], while for the V and Cr groups compounds there is an alternation of the lowest energy phase. The V group compounds have a small energy difference between the phases, which is manifested with the synthesis of 2H and 1T phases among these materials [7], and 2H is the most stable for compounds with S and Se whereas 1T$_d$ is the most stable for compounds with Te. Compounds with V are experimentally observed in the 2H phase, in contrast with our results, however it has been shown that due to the small energy difference between the phases, temperature effects might change the lowest energy phase, in agreement with the synthesis of 1T-$VS_2$ at room temperature [47].

In Cr group, 2H predominates as the lowest energy phase ($MoQ_2$, $WS_2$, $WSe_2$), as expected [5]. The exceptions are $CrSe_2$ (1T), $CrTe_2$ (1T), and $WTe_2$ (1T$_d$), which were all experimentally observed crystal structures [7,48,49]. Finally, the room temperature crystal structures of $NbTe_2$ and $TaTe_2$, which are formed of a monoclinic lattice [50], are not considered in our calculations. However, among the structures considered, the 1T$_d$ phase, that has the same intra-layer structural configuration of distorted octahedral coordination

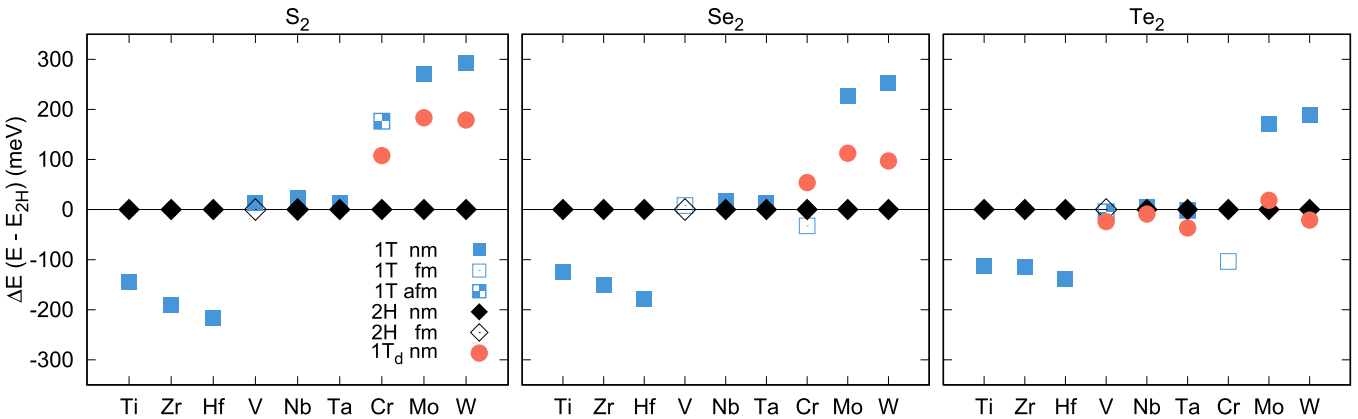


FIG. 2. Relative total energy between 1T, 1T$_d$, and 2H phases for $MS_2$, $MSe_2$, and $MTe_2$, where $M$ is the metal indicated in the $x$ axis. 2H phase is used as reference, so the vertical axis presents the values for $(E_{(1T,1T_d,2H)} - E_{2H})$. The magnetic ordering is indicated by the symbols in the key: nonmagnetic (nm), ferromagnetic (fm), and antiferromagnetic (afm).

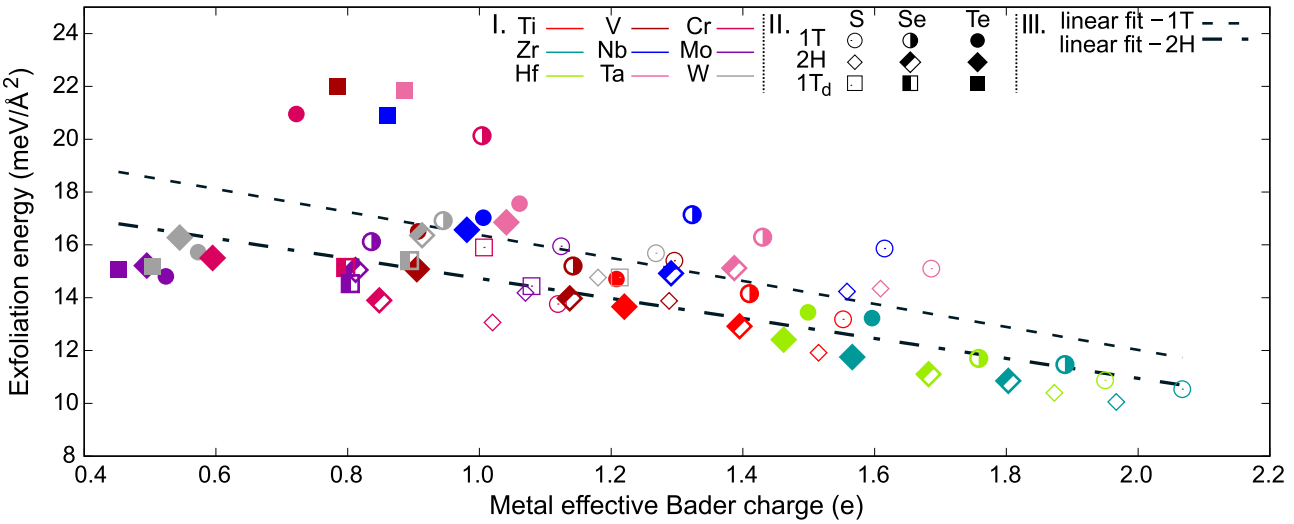


FIG. 3. Exfoliation energy as function of the metal effective Bader charge. Compounds can be identified by the combination of the color in Legend I with the symbol in Legend II. Legend III presents the key for the linear fitting of phases 1T and 2H.

of metal atoms, was obtained as the lowest energy one for these compounds.

Therefore, our results are in line with the general rule of the strong influence of the filling of metal *d* orbitals on the lowest energy phase of each compound [5,12], as can be seen in the preference of 1T phase for Ti group compounds, and mostly 2H phase for TMDs of V and Cr groups. However, other effects are important to determine the energetic favored phase, like magnetism. From our results, only the V group and Cr compounds favor a magnetic ordering, depending on the phase: $VS_2$, $VSe_2$, $VTe_2$, and $NbS_2$ in 2H phase are ferromagnetic, as well as $VSe_2$ and $TaTe_2$ in 1T phase, while $CrS_2$ and $VTe_2$ in 1T phase are antiferromagnetic. This information is also presented in Fig. 2. A recent theoretical work [23] reported that the 1T monolayers of V dichalcogenides are ferromagnetic, and 1T-$CrSe_2$ monolayer is reported as antiferromagnetic.

The antiferromagnetic ordering was also obtained by experimental measurements in bulk 1T-$CrSe_2$ [48], although we obtained lower energy for the ferromagnetic ordering. The energy difference between the two orderings in our calculations, however, is of only 4 meV, i.e., the phases are approximately degenerate and stable. Furthermore, this difference is so small that, the use of a different vdW correction may change the result, also considering that variations on the *c* lattice parameter were shown to modify the energetic preference between the two orderings [48]. The relative energies for all magnetic configurations are presented in the Supplemental Material [42].

### B. Exfoliation energy

To investigate the strength of interlayer binding in TMDs and determine how easily they can be exfoliated, we calculated the exfoliation energy. As the polymorphic structures have different unit cells, we calculate exfoliation energies per monolayer area in the unit cell. In Fig. 3, the exfoliation energy is shown as a function of metal effective Bader charge [51,52], i.e., an estimate of the charge transfer from metal to chalcogen atoms. Several works, using different levels of vdW corrections [23,53–56], propose a classification of the materials that are easily or potentially exfoliable based on the exfoliation energy. We adopt the classification in which materials with exfoliation energy of 15 to 20 meV/Å$^2$ are considered easily exfoliable, while materials with energies above these values up to 130 meV/Å$^2$ are considered potentially exfoliable.

In our results, almost all the studied compounds have exfoliation energies in the range of 10 to 17 meV/Å$^2$ and can be classified as easily exfoliable, as shown in Fig. 3. The exceptions are: (i) $CrSe_2$ and $CrTe_2$ in the 1T phase, with 20 and 21 meV/Å$^2$, respectively; (ii) $VTe_2$, $TaTe_2$, and $NbTe_2$ in the 1T$_d$ phase, with 22, 22, and 21 meV/Å$^2$, respectively.

An analysis of Fig. 3 shows that the exfoliation energy decreases linearly with the increase of the metal effective Bader charge, presenting a clear trend. This relation arises because with the increase of the charge on metal atoms, and consequently with the increase of the magnitude of the charge on the chalcogen plane, the effective Coulomb repulsion among the layers also increases, resulting in larger interlayer distances and smaller exfoliation energies. There is a small difference between polymorphic phases, as indicated by the separate linear fittings in Fig. 3, which may be related to the atom ordering in the chalcogen plane. As generally 1T phase has higher in-plane lattice parameters when compared with 2H, less charge is accumulated in the chalcogen plane in 1T than in 2H. As a result, the distance between planes is smaller and the exfoliation energy is larger. Nevertheless, this difference is small, as shown for 2H and 1T $ZrS_2$ in Fig. 3. When the charge transfer is lower, Coulomb repulsion plays a smaller role, leading the exfoliation energies to be more dependent on other effects, e.g., van der Waals interaction, causing larger deviations from the linear trend, as with the cases of stronger (>20 meV/Å$^2$) interlayer binding. Thus, the linear correlation is not clear for 1T$_d$, which may be due to the nonuniformities in the chalcogen plane caused by the distortions typical of this phase. All values of exfoliation energy and Bader charge are available in Supplemental Material [42].

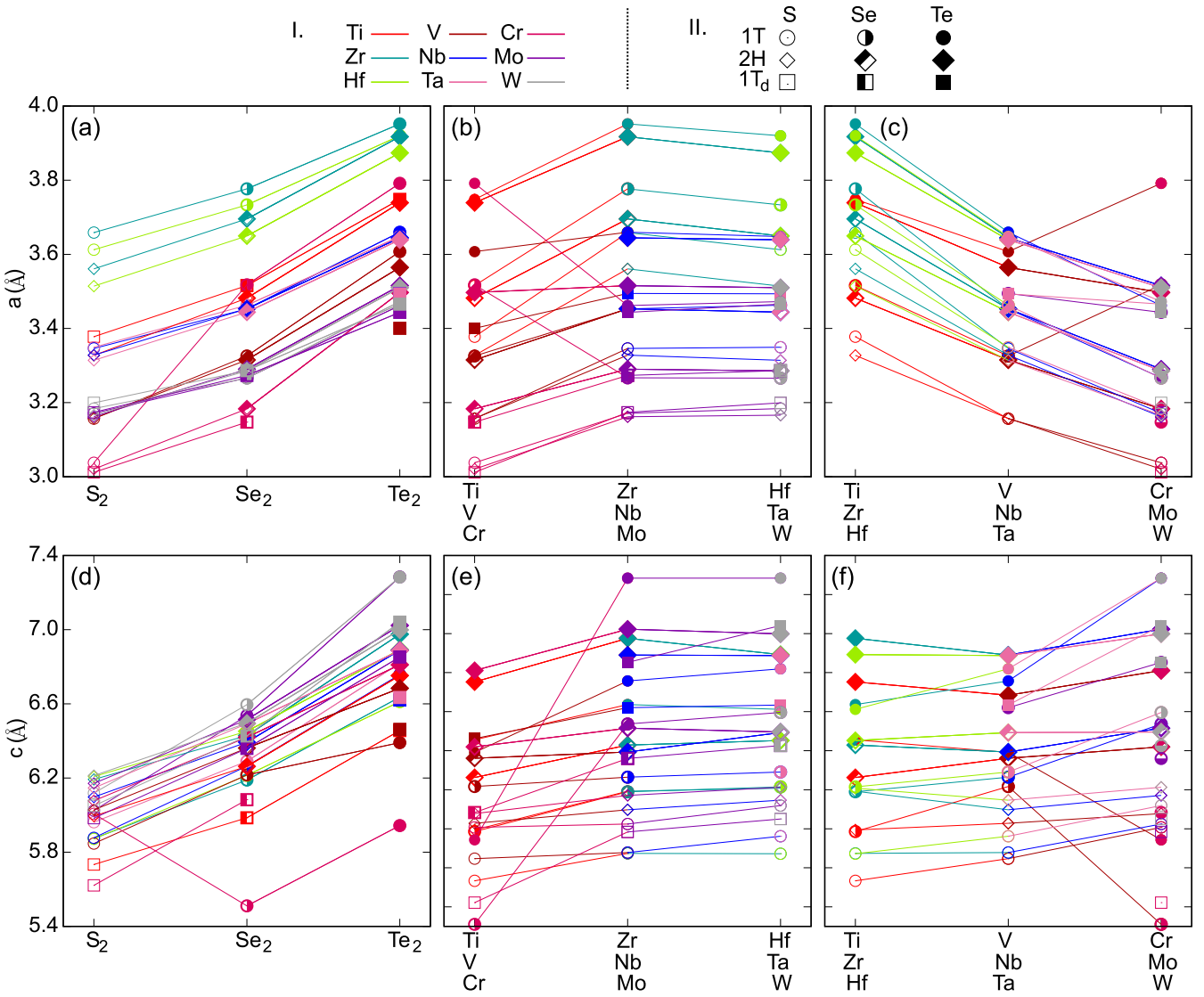


FIG. 4. Lattice parameters of the 2H, 1T, and 1T$_d$ TMDs. Compounds are identified by the combination of the color, in Legend I, with the symbols, in Legend II. The out-of-plane lattice parameter is normalized by the number of layers in the unit cell. In (a) and (d) the dependence on the chalcogen species is shown, (b) and (e) present the dependence on the transition metal period, and (c) and (f) show the dependence on the metal group. All numerical values are presented in the Supplemental Material [42].

### C. Equilibrium volume

In Fig. 4, we show in-plane, $a$, and perpendicular, $c$, lattice parameters. Due to the different number of layers in the unit cells between the polymorphs, in order to compare all the materials, we used the value of the out-of-plane lattice parameter divided by the number of layers to obtain $c$. As expected, the lattice parameters increase monotonically with the chalcogen atomic radius (covalent radius reference values are 1.04 Å, 1.14 Å, and 1.32 Å for S, Se, Te, respectively [57]), as shown in Figs. 4(a) and 4(d). The exceptions are the 1T Cr compounds that present an abnormal increase of $c$ from $CrSe_2$ to $CrS_2$.

The effect of varying transition-metal period, with fixed metal group and chalcogen species, on the lattice parameters is represented in Figs. 4(b) and 4(e). Compounds with transition-metal belonging to period 4 (Ti, V, and Cr) have the smallest parameters, while compounds with transition metals belonging to periods 5 (Zr, Nb, and Mo) and 6 (Hf, Ta, and W) have similar lattice parameters. This is also in agreement with the trend of atomic radii of the transition metals, which are the smallest for transition metals belonging to period 4 and have closer values for transition metals from periods 5 and 6, for example 1.28 Å, 1.40 Å and 1.41 Å for Cr, Mo, and W, respectively [57].

The atomic radii of transition metals (e.g., 1.46 Å, 1.35, Å and 1.28 Å for Ti, V, and Cr, respectively [57]) also determine the decrease of the parameter $a$ with the increase of the column number of the transition metal group, for a fixed period and a chalcogen species, as shown in Fig. 4(c). There is no clearly defined trend for the $c$ parameter. Compared with the experimental data for the already synthesized TMDs, as showed in the Table I, the calculated lattice parameters present mean absolute percentage errors (MAPE) lower than 1% for in-plane lattice parameters ($a$ and $b$) and lower than 2% for the perpendicular lattice parameter ($c$), indicating that PBE-D3 predicts reasonable values for vdW effects in TMDs.

TABLE I. Lattice parameters obtained from DFT, compared to their experimental values. Materials that are unstable in the phase $1T_d$ are indicated. The experimental values were extracted from Ref. [10]. All values are presented in Å.

| | Phase | | $a_0$ | $b_0$ | $c_0$ | | Phase | | $a_0$ | $b_0$ | $c_0$ | | Phase | | $a_0$ | $b_0$ | $c_0$ |
|---|---|---|---|---|---|---|---|---|---|---|---|---|---|---|---|---|---|
| $TiS_2$ | 2H | DFT | 3.33 | 3.33 | 11.99 | $TiSe_2$ | 2H | DFT | 3.48 | 3.48 | 12.51 | $TiTe_2$ | 2H | DFT | 3.73 | 3.73 | 13.50 |
| | 1T | | 3.38 | 3.38 | 5.73 | | 1T | | 3.51 | 3.51 | 5.98 | | 1T | | 3.74 | 3.74 | 6.45 |
| | $1T_d$ | | | Unstable | | | $1T_d$ | | | Unstable | | | $1T_d$ | | | Unstable | |
| | 1T | Exp. | 3.41 | 3.41 | 5.70 | | 1T | Exp. | 3.53 | 3.53 | 6.00 | | 1T | Exp. | 3.76 | 3.76 | 6.52 |
| $ZrS_2$ | 2H | DFT | 3.56 | 3.56 | 12.38 | $ZrSe_2$ | 2H | DFT | 3.69 | 3.69 | 12.85 | $ZrTe_2$ | 2H | DFT | 3.91 | 3.91 | 13.95 |
| | 1T | | 3.65 | 3.65 | 5.87 | | 1T | | 3.77 | 3.77 | 6.18 | | 1T | | 3.95 | 3.95 | 6.63 |
| | $1T_d$ | | | Unstable | | | $1T_d$ | | | Unstable | | | $1T_d$ | | | Unstable | |
| | 1T | Exp. | 3.66 | 3.66 | 5.81 | | 1T | Exp. | 3.77 | 3.77 | 6.13 | | 1T | Exp. | 3.95 | 3.95 | 6.63 |
| $HfS_2$ | 2H | DFT | 3.51 | 3.51 | 12.41 | $HfSe_2$ | 2H | DFT | 3.64 | 3.64 | 12.90 | $HfTe_2$ | 2H | DFT | 3.87 | 3.87 | 13.78 |
| | 1T | | 3.61 | 3.61 | 5.87 | | 1T | | 3.73 | 3.73 | 6.21 | | 1T | | 3.91 | 3.91 | 6.61 |
| | $1T_d$ | | | Unstable | | | $1T_d$ | | | Unstable | | | $1T_d$ | | | Unstable | |
| | 2H | Exp. | 3.37 | 3.37 | 11.78 | | 2H | Exp. | 3.44 | 3.44 | 12.38 | | 2H | Exp. | | | |
| | 1T | | 3.95 | 3.95 | 6.65 | | 1T | | 3.74 | 3.74 | 6.14 | | 1T | | 3.95 | 3.95 | 6.65 |
| $VS_2$ | 2H | DFT | 3.15 | 3.15 | 12.05 | $VSe_2$ | 2H | DFT | 3.31 | 3.31 | 12.72 | $VTe_2$ | 2H | DFT | 3.56 | 3.56 | 13.36 |
| | 1T | | 3.15 | 3.15 | 5.84 | | 1T | | 3.32 | 3.32 | 6.21 | | 1T | | 3.60 | 3.60 | 6.39 |
| | $1T_d$ | | | Unstable | | | $1T_d$ | | | Unstable | | | $1T_d$ | | 3.40 | 6.42 | 6.46 |
| | 1T | Exp. | | | | | 1T | Exp. | 3.34 | 3.34 | 6.12 | | 1T | Exp. | | | |
| $NbS_2$ | 2H | DFT | 3.33 | 3.33 | 12.18 | $NbSe_2$ | 2H | DFT | 3.45 | 3.45 | 12.78 | $NbTe_2$ | 2H | DFT | 3.64 | 3.64 | 13.76 |
| | 1T | | 3.34 | 3.34 | 5.87 | | 1T | | 3.45 | 3.45 | 6.26 | | 1T | | 3.65 | 3.65 | 6.76 |
| | $1T_d$ | | | Unstable | | | $1T_d$ | | | Unstable | | | $1T_d$ | | 3.49 | 6.75 | 6.62 |
| | 2H | Exp. | 3.31 | 3.31 | 11.88 | | 2H | Exp. | 3.44 | 3.44 | 12.55 | | 2H | Exp. | | | |
| | 1T | | | | | | 1T | | 3.53 | 3.53 | 6.29 | | 1T | | | | |
| $TaS_2$ | 2H | DFT | 3.32 | 3.32 | 12.16 | $TaSe_2$ | 2H | DFT | 3.44 | 3.44 | 12.98 | $TaTe_2$ | 2H | DFT | 3.32 | 3.32 | 11.98 |
| | 1T | | 3.34 | 3.34 | 5.96 | | 1T | | 3.46 | 3.46 | 6.29 | | 1T | | 3.64 | 3.64 | 6.81 |
| | $1T_d$ | | | Unstable | | | $1T_d$ | | | Unstable | | | $1T_d$ | | 3.49 | 6.68 | 6.63 |
| | 2H | Exp. | 3.31 | 3.31 | 12.10 | | 2H | Exp. | 3.43 | 3.43 | 12.72 | | 2H | Exp. | | | |
| | 1T | | 3.36 | 3.36 | 5.90 | | 1T | | 3.47 | 3.47 | 6.27 | | 1T | | | | |
| $CrS_2$ | 2H | DFT | 3.02 | 3.02 | 12.15 | $CrSe_2$ | 2H | DFT | 3.18 | 3.18 | 12.83 | $CrTe_2$ | 2H | DFT | 3.49 | 3.49 | 13.62 |
| | 1T | | 3.31 | 3.31 | 5.34 | | 1T | | 3.51 | 3.51 | 5.51 | | 1T | | 3.79 | 3.79 | 5.94 |
| | $1T_d$ | | 3.01 | 5.53 | 5.62 | | $1T_d$ | | 3.14 | 5.75 | 6.08 | | $1T_d$ | | | Unstable | |
| $MoS_2$ | 2H | DFT | 3.16 | 3.16 | 12.34 | $MoSe_2$ | 2H | DFT | 3.29 | 3.29 | 13.03 | $MoTe_2$ | 2H | DFT | 3.51 | 3.51 | 14.04 |
| | 1T | | 3.17 | 3.17 | 6.02 | | 1T | | 3.26 | 3.26 | 6.53 | | 1T | | 3.46 | 3.46 | 7.28 |
| | $1T_d$ | | 3.17 | 5.71 | 5.98 | | $1T_d$ | | 3.27 | 5.94 | 6.35 | | $1T_d$ | | 3.44 | 6.37 | 6.85 |
| | 2H | Exp. | 3.15 | 3.15 | 12.29 | | 2H | Exp. | 3.29 | 3.29 | 12.90 | | 2H | Exp. | 3.51 | 3.51 | 13.97 |
| $WS_2$ | 2H | DFT | 3.16 | 3.16 | 12.42 | $WSe_2$ | 2H | DFT | 3.28 | 3.28 | 12.99 | $WTe_2$ | 2H | DFT | 3.50 | 3.50 | 13.99 |
| | 1T | | 3.18 | 3.18 | 6.11 | | 1T | | 3.26 | 3.26 | 6.59 | | 1T | | 3.37 | 3.37 | 5.73 |
| | $1T_d$ | | 3.19 | 5.70 | 6.05 | | $1T_d$ | | 3.28 | 5.92 | 6.42 | | $1T_d$ | | 3.46 | 6.27 | 7.04 |
| | 2H | Exp. | 3.17 | 3.17 | 12.36 | | 2H | Exp. | 3.28 | 3.28 | 12.95 | | $1T_d$ | Exp. | 3.477 | 6.25 | 7.01 |

### D. Elastic constants

As we consider some compositions and polymorphic phases not yet synthesized, the structural stability of the materials was addressed by the Born elastic stability criteria [58], and hence, we analyzed the stability of the TMDs through the evaluation of the elastic constants and verification of the Born elastic stability criteria as discussed by Mouhat and Coudert [59]. Due to their symmetry, the crystals of 1T, 2H, and $1T_d$ phases present 6, 5, and 9 nonzero and independent elastic constants, respectively, which must satisfy the necessary and sufficient conditions for stability discussed below.

For the 1T phase ($P\bar{3}m1$ space group), with elastic constants $C_{11}$, $C_{12}$, $C_{13}$, $C_{14}$, $C_{33}$, and $C_{44}$ [and $C_{66} = (C_{11} - C_{12})/2$], the conditions are

$$\begin{aligned} &C_{11} > |C_{12}|, \quad C_{44} > 0, \\ &C_{13}^2 < \tfrac{1}{2}C_{33}(C_{11} + C_{12}), \\ &C_{14}^2 < \tfrac{1}{2}C_{44}(C_{11} - C_{12}). \end{aligned} \tag{1}$$

For the crystal of 2H phase ($P6_3/mmc$ space group), that has the elastic constants $C_{11}, C_{12}, C_{13}, C_{33}, C_{44}$ [with $C_{66} = (C_{11} - C_{12})/2$], the conditions are

$$C_{11} > |C_{12}|, \quad C_{13}^2 < \tfrac{1}{2}C_{33}(C_{11} + C_{12}), \quad C_{44} > 0. \tag{2}$$

Finally, the elastic constants of the $1T_d$ phase crystal ($Pnm2_1$ space group), $C_{11}$, $C_{12}$, $C_{13}$, $C_{22}$, $C_{23}$, $C_{33}$, $C_{44}$, $C_{55}$, and $C_{66}$, must satisfy the following conditions:

$$\begin{aligned} &\left[C_{11}C_{22}C_{33} + 2C_{12}C_{13}C_{23} - C_{11}C_{23}^2 \right. \\ &\quad \left. - C_{22}C_{13}^2 - C_{33}C_{12}^2\right] > 0, \\ &C_{11}C_{12} > C_{12}^2, \quad C_{11} > 0, \quad C_{44} > 0, \\ &C_{55} > 0, \quad C_{66} > 0. \end{aligned} \tag{3}$$

All the elastics constants values are shown in the Supplemental Material [42], while the diagonal elastic constants are shown in Fig. 5. We found that all conditions for the elastic

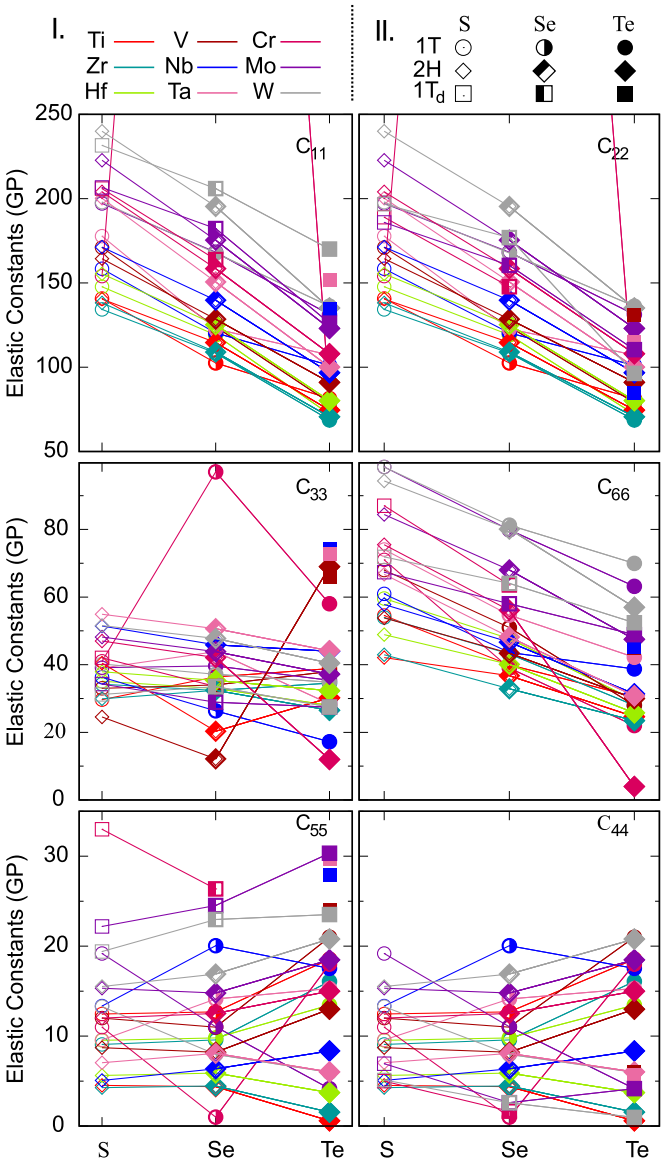


FIG. 5. Diagonal elements of the elastic matrix of the 1T, 2H, and 1T$_d$ TMD bulks.

stability are satisfied, and hence, those configurations are local minimum structures. Our results are in agreement with previous calculations [60] and experimental results [7,61]. For the elastic constants $C_{11}$ and $C_{22}$, which are not related to the out of plane direction ($z$), the magnitude decreases with the chalcogen radius and have higher values when compared with the other elastic constants, as shown in Fig. 5. This occurs because in plane binding, that is dominated by covalent bonds, is weaker for larger chalcogen radius, and is stronger than the out of plane van der Waals interactions. Therefore, the other elastic constants, which are related to the $z$ direction, have a smaller magnitude, and present deviant trends for the chalcogen radius, due to the role of the van der Waals interactions in the interlayer interactions.

### E. Band structure and density of states

To characterize the materials according to their electronic properties, we calculated the band structure and the density of states of the 64 stable TMDs with the hybrid functional HSE06. The results for 2H-phase selenides of the 3$d$-metals are shown in Fig. 6, and the results for the other systems are in the Supplemental Material [42]. From the analysis of the results, the materials were classified as metals, semi-metals or semiconductors, as indicated in Fig. 7. Among all the studied TMDs, 22 were identified as semiconductors, with band gaps ranging from 0.20 to 1.75 eV.

In the literature, works that estimate the band gaps for TMDs in the bulk phase mainly use the crystal structures acquired from crystallographic databases [62,63] presenting band gap values that differ from our results. The difference of values is due to the use of the PBE functional, that is known to underestimate the band gap [33,38,64]. In Table II, we present the values of PBE, PBE+SOC, HSE06 and experimental band gaps for the TMD semiconductor materials. The comparison of PBE and PBE+SOC shows that the inclusion of SOC modify the gap values usually from less than one to a few decades of meV, exception made for $ZrSe_2$-1T, $HfSe_2$-1T, and $WTe_2$-2H where this difference is about 150 meV. However, the PBE functional usually underestimates the gap in the order of several hundreds of meVs. Despite the absence of the

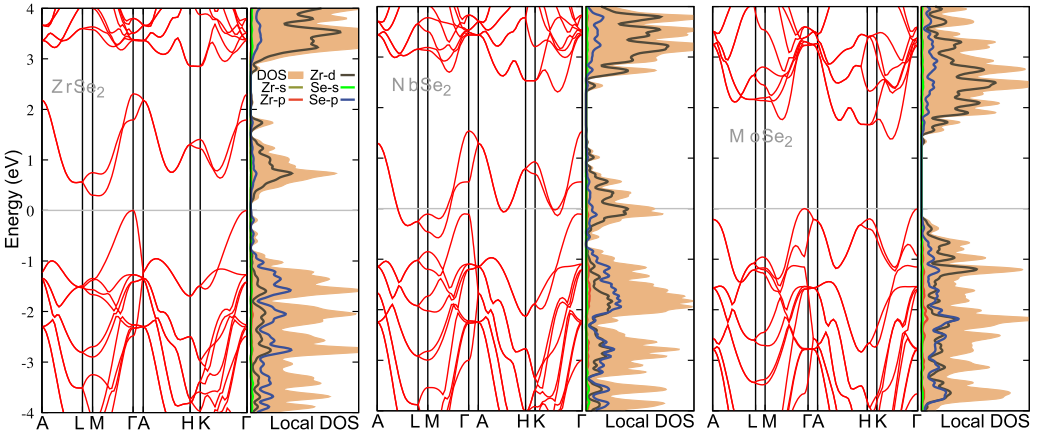


FIG. 6. 2H-phase DFT-HSE06 band structures and densities of states of $ZrSe_2$ (left), $NbSe_2$ (center), and $MoSe_2$ (right). Vertical lines indicate high-symmetry points in the first Brillouin zone. At the right panels, shadowed curves indicate the density of states (DOS) while the solid lines indicate the local density of states in $s$-, $p$-, and $d$-orbitals of each atomic species.

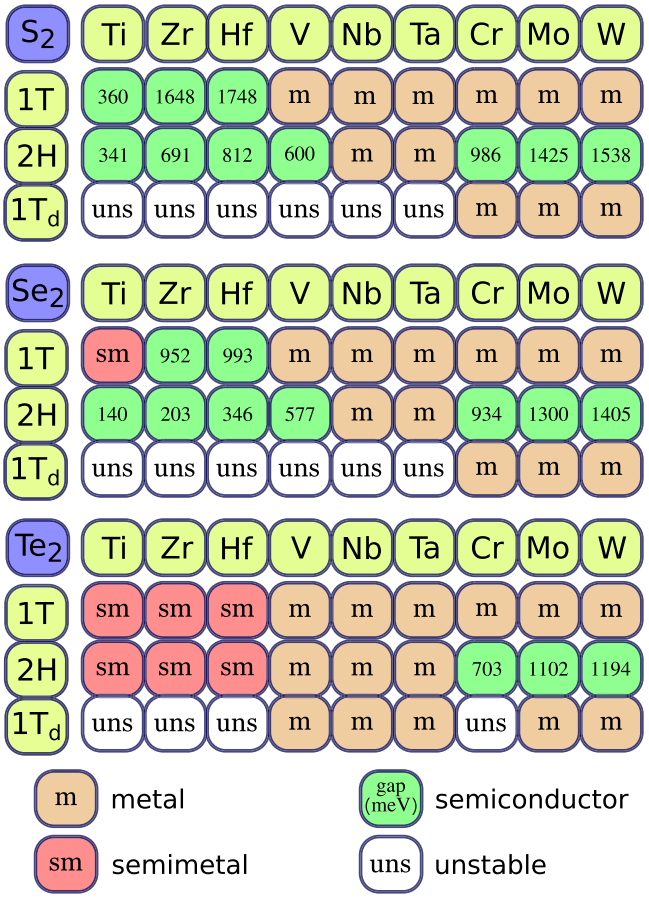


FIG. 7. Classification of stable material phases according to their electronic band gap: metal (m), semimetal (sm), or semiconductor. In semiconductors, predicted gap energy values are shown in meV units. Unstable phases are indicated by (uns).

SOC corrections on the HSE06 calculations this functional shows more realistic band gaps when compared with the experimentally measured values, preventing the high computational costs associated to the combined use of HSE06 and SOC.

For each phase and considering compositions with the same chalcogen, the transition metal $d$ electron count determines the electronic character of the material. For example, in 2H-$MSe_2$ compounds, as shown in Fig. 6, with the progressive filling of the $d$ band from Zr to Nb to Mo $ZrSe_2$ is a semiconductor, while $NbSe_2$ is a metal, and the band is fully occupied in $MoSe_2$, recovering the semiconductor character. Therefore, if the $d$-orbitals are completely occupied or empty, then the TMDs have semiconducting behavior, while if the $d$-orbitals have the partial occupation, then the TMDs have conducting behavior. These results are in agreement with other reports in the literature [11,12]. Because the crystal symmetry, i.e., the polymorphic phase, strongly affects the energy of the $d$ bands, the same compound can have different electronic properties depending on the polymorphic phase. For example, $MoS_2$ is metallic in the 1T phase, but is a semiconductor in the 2H phase [16,17].

TABLE II. PBE, PBE with spin-orbit coupling (PBE+SOC), HSE06 and experimental band gaps for TMD semiconductor materials. All energies are given in meV.

| Material | Phase | PBE | PBE+SOC | HSE06 | Exp. |
|---|---|---|---|---|---|
| $TiS_2$ | 1T | 0 | 15 | 360 | |
| $ZrS_2$ | 1T | 848 | 850 | 1648 | |
| $ZrSe_2$ | 1T | 260 | 109 | 952 | |
| $HfS_2$ | 1T | 988 | 974 | 1748 | |
| $HfSe_2$ | 1T | 378 | 203 | 993 | |
| $TiS_2$ | 2H | 0 | 0 | 341 | |
| $TiSe_2$ | 2H | 0 | 0 | 140 | |
| $ZrS_2$ | 2H | 0 | 0 | 691 | |
| $ZrSe_2$ | 2H | 0 | 0 | 203 | |
| $HfS_2$ | 2H | 159 | 172 | 812 | |
| $HfSe_2$ | 2H | 0 | 0 | 346 | |
| $VS_2$ | 2H | 0 | 0 | 600 | |
| $VSe_2$ | 2H | 0 | 0 | 577 | |
| $CrS_2$ | 2H | 604 | 600 | 986 | |
| $CrSe_2$ | 2H | 600 | 589 | 934 | |
| $CrTe_2$ | 2H | 327 | 313 | 703 | |
| $MoS_2$ | 2H | 918 | 912 | 1425 | 1230[b] |
| $MoSe_2$ | 2H | 870 | 860 | 1300 | 1090[b] |
| $MoTe_2$ | 2H | 739 | 720 | 1102 | 880[a] |
| $WS_2$ | 2H | 1040 | 990 | 1538 | 1350[b] |
| $WSe_2$ | 2H | 959 | 882 | 1405 | 1200[b] |
| $WTe_2$ | 2H | 757 | 603 | 1194 | |

[a]Scanning tunneling spectroscopy and ionic-liquid gated transistors at room temperature [65].
[b]Photocurrent spectra at room temperature [66].

Band gaps vary with the composition in a similar way for the three studied phases. The increase in chalcogen atomic number narrows the band gap, because the energy of $Q$-$p$ derived states, which compose the valence band maximum, is increased. For semiconductors with the same phase and chalcogen, the band gap increases with the transition metal atomic number, e.g., $TiQ_2^{gap} < ZrQ_2^{gap} < HfQ_2^{gap}$ in phase 1T, as shown in Fig. 7. This trend occurs due to the localization of the $d$ orbitals, since their energy difference from the Fermi energy increases, i.e., looking for compounds with the same phase, the $d$-orbitals in $TiS_2$ have energies closer to Fermi energy than those in $ZrS_2$.

## V. CONCLUSION

We investigated 27 TMD bulk compounds obtained by the combination of nine transition-metals (Ti, Zr, Hf, V, Nb, Ta, Cr, Mo, and W) with three chalcogens (S, Se, and Te) in three polymorphic phases, namely, 1T, 2H, and $1T_d$. We obtained the equilibrium geometry configuration and the lowest energy phase for each material, which are in good agreement with experimental data for the already synthesized compositions. The magnetic ordering was also addressed, and some of the materials with transition-metal from the V group and compounds with Cr showed ferromagnetic or antiferromagnetic behavior. The effects of chemical composition on the equilibrium lattice parameters mostly follow the expected trends based on the atomic radius.

To investigate the stability of the crystal structures, we obtained the elastic constants and employed the Born elastic stability criteria, which was satisfied for all the systems. The exfoliation energy of all stable materials was calculated, indicating that the majority of the studied TMDs have weak interlayer binding and therefore are predicted as easy to exfoliate in order to obtain their two-dimensional form. We found that the increase of the charge transfer within each layer decreases the magnitude of the exfoliation energy, due to the Coulomb repulsion between chalcogen planes. The electronic band structure and density of states were calculated, which allowed classifying the materials like metal, semimetal or semiconductor, according to their band gap. We demonstrated that the occupation of metal *d* band determines the electronic character of the material. This study provides a comprehensible understanding of the properties of layered TMDs in different polymorphic phases, including material not yet synthesized, and therefore can contribute to further development of layered and two-dimensional materials based on TMDs.

## ACKNOWLEDGMENTS

The authors gratefully acknowledge support from FAPESP (São Paulo Research Foundation, Grant No. 2017/11631-2), Shell and the strategic importance of the support given by ANP (Brazil's National Oil, Natural Gas and Biofuels Agency) through the R&D levy regulation. R.B. acknowledges financial support (Ph.D. fellowship) from FAPESP, Grant No. 2017/09077-7. This study was financed in part by the Coordenação de Aperfeiçoamento de Pessoal de Nível Superior-Brasil (CAPES)-Finance Code 001. G.M.S. acknowledges CAPES-CsF (Grant No. 88881.068174/2014-01) and CNPq (Grants No. 304289/2015-9 and No. 308806/2018-2).

[1] J. Wilson and A. Yoffe, Adv. Phys. **18**, 193 (1969).
[2] F. J. Clauss, *Solid Lubricants and Self-Lubricating Solids* (Elsevier, Amsterdam, 1972).
[3] M. S. Whittingham, Chem. Rev. **104**, 4271 (2004).
[4] R. Lv, J. A. Robinson, R. E. Schaak, D. Sun, Y. Sun, T. E. Mallouk, and M. Terrones, Acc. Chem. Res. **48**, 56 (2014).
[5] M. Chhowalla, H. S. Shin, G. Eda, L.-J. Li, K. P. Loh, and H. Zhang, Nat. Chem. **5**, 263 (2013).
[6] A. K. Geim and K. S. Novoselov, Nat. Mater. **6**, 183 (2007).
[7] A. V. Kolobov and J. Tominaga, *Two-Dimensional Transition-Metal Dichalcogenides* (Springer International Publishing, Berlin, 2016).
[8] L. Peng, Y. Yuan, G. Li, X. Yang, J.-J. Xian, C.-J. Yi, Y.-G. Shi, and Y.-S. Fu, Nat. Commun. **8**, 65 (2017).
[9] K. Deng, G. Wan, P. Deng, K. Zhang, S. Ding, E. Wang, M. Yan, H. Huang, H. Zhang, Z. Xu, J. Denlinger, A. Fedorov, H. Yang, W. Duan, H. Yao, Y. Wu, S. Fan, H. Zhang, X. Chen, and S. Zhou, Nat. Phys. **12**, 1105 (2016).
[10] F. Hulliger and F. Lévy, *Structural Chemistry of Layer-Type Phases*, 1st ed., Physics and Chemistry of Materials with Layered Structures 5 (Springer, Netherlands, 1977).
[11] D. Voiry, A. Mohite, and M. Chhowalla, Chem. Soc. Rev. **44**, 2702 (2015).
[12] H. Yang, S. W. Kim, M. Chhowalla, and Y. H. Lee, Nat. Phys. **13**, 931 (2017).
[13] R. Besse, N. A. M. S. Caturello, C. M. O. Bastos, D. Guedes-Sobrinho, M. P. Lima, G. M. Sipahi, and J. L. F. D. Silva, J. Phys. Chem. C **122**, 20483 (2018).
[14] D. H. Keum, S. Cho, J. H. Kim, D.-H. Choe, H.-J. Sung, M. Kan, H. Kang, J.-Y. Hwang, S. W. Kim, H. Yang, K. J. Chang, and Y. H. Lee, Nat. Phys. **11**, 482 (2015).
[15] S. Cho, S. Kim, J. H. Kim, J. Zhao, J. Seok, D. H. Keum, J. Baik, D.-H. Choe, K. J. Chang, K. Suenaga, S. W. Kim, Y. H. Lee, and H. Yang, Science **349**, 625 (2015).
[16] F. Wypych and R. Schöllhorn, J. Chem. Soc., Chem. Commun. **0**, 1386 (1992).
[17] Q. Tang and D. en Jiang, Chem. Mater. **27**, 3743 (2015).
[18] S. L. Wong, H. Liu, and D. Chi, Prog. Cryst. Growth Charact. Mater. **62**, 9 (2016).
[19] H. C. Diaz, Y. Ma, R. Chaghi, and M. Batzill, Appl. Phys. Lett. **108**, 191606 (2016).
[20] T. A. J. Loh, D. H. C. Chua, and A. T. S. Wee, Sci. Rep. **5**, 18116 (2015).
[21] L. K. Tan, B. Liu, J. H. Teng, S. Guo, H. Y. Low, and K. P. Loh, Nanoscale **6**, 10584 (2014).
[22] K. S. Novoselov, D. Jiang, F. Schedin, T. J. Booth, V. V. Khotkevich, S. V. Morozov, and A. K. Geim, Proc. Natl. Acad. Sci. USA **102**, 10451 (2005).
[23] N. Mounet, M. Gibertini, P. Schwaller, D. Campi, A. Merkys, A. Marrazzo, T. Sohier, I. E. Castelli, A. Cepellotti, G. Pizzi, and N. Marzari, Nat. Nanotechnol. **13**, 246 (2018).
[24] P. Hohenberg and W. Kohn, Phys. Rev. **136**, B864 (1964).
[25] W. Kohn and L. J. Sham, Phys. Rev. **140**, A1133 (1965).
[26] J. P. Perdew, K. Burke, and M. Ernzerhof, Phys. Rev. Lett. **77**, 3865 (1996).
[27] P. E. Blöchl, Phys. Rev. B **50**, 17953 (1994).
[28] G. Kresse and J. Hafner, Phys. Rev. B **48**, 13115 (1993).
[29] G. Kresse and J. Furthmüller, Phys. Rev. B **54**, 11169 (1996).
[30] T. Tsuneda, *Density Functional Theory in Quantum Chemistry* (Springer Nature, Berlin, 2014).
[31] S. Grimme, J. Antony, S. Ehrlich, and H. Krieg, J. Chem. Phys. **132**, 154104 (2010).
[32] H. Peelaers and C. G. V. de Walle, J. Phys.: Condens. Matter **26**, 305502 (2014).
[33] J. P. Perdew and A. Zunger, Phys. Rev. B **23**, 5048 (1981).
[34] R. G. Parr and Y. Weitao, *Density-Functional Theory of Atoms and Molecules (International Series of Monographs on Chemistry)* (Oxford University Press, Oxford, 1994).
[35] P. Mori-Sánchez, A. J. Cohen, and W. Yang, Phys. Rev. Lett. **100**, 146401 (2008).
[36] Y.-S. Kim, K. Hummer, and G. Kresse, Phys. Rev. B **80**, 035203 (2009).
[37] E. Engel and R. M. Dreizler, *Density Functional Theory* (Springer, Berlin/Heidelberg, 2011).
[38] C. M. O. Bastos, F. P. Sabino, G. M. Sipahi, and J. L. F. D. Silva, J. Appl. Phys. **123**, 065702 (2018).
[39] J. Heyd, G. E. Scuseria, and M. Ernzerhof, J. Chem. Phys. **118**, 8207 (2003).

[40] J. Heyd, G. E. Scuseria, and M. Ernzerhof, J. Chem. Phys. **124**, 219906 (2006).
[41] D. D. Koelling and B. N. Harmon, J. Phys. C: Solid State Phys. **10**, 3107 (1977).
[42] See Supplemental Material at http://link.aps.org/supplemental/10.1103/PhysRevMaterials.3.044002 for computational details, convergence tests, initial magnetic configurations, relative energies, elastic constants, exfoliation energies, band structures, and density of states of the materials described in this article.
[43] Y. LePage and P. Saxe, Phys. Rev. B **65**, 104104 (2002).
[44] X. Wu, D. Vanderbilt, and D. R. Hamann, Phys. Rev. B **72**, 035105 (2005).
[45] H. J. Monkhorst and J. D. Pack, Phys. Rev. B **13**, 5188 (1976).
[46] D. Gao, Q. Xue, X. Mao, W. Wang, Q. Xu, and D. Xue, J. Mater. Chem. C **1**, 5909 (2013).
[47] H. Zhang, L.-M. Liu, and W.-M. Lau, J. Mater. Chem. A **1**, 10821 (2013).
[48] D. C. Freitas, M. Núñez, P. Strobel, A. Sulpice, R. Weht, A. A. Aligia, and M. Núñez-Regueiro, Phys. Rev. B **87**, 014420 (2013).
[49] D. C. Freitas, R. Weht, A. Sulpice, G. Remenyi, P. Strobel, F. Gay, J. Marcus, and M. Núñez-Regueiro, J. Phys.: Condens. Matter **27**, 176002 (2015).
[50] B. E. Brown, Acta Crystallogr. **20**, 264 (1966).
[51] R. F. W. Bader, *Atoms in Molecules: A Quantum Theory*, International Ser. of Monogr. on Chem (Clarendon Press, Oxford, 1994).
[52] W. Tang, E. Sanville, and G. Henkelman, J. Phys.: Condens. Matter **21**, 084204 (2009).
[53] T. Björkman, A. Gulans, A. V. Krasheninnikov, and R. M. Nieminen, Phys. Rev. Lett. **108**, 235502 (2012).
[54] T. Björkman, A. Gulans, A. V. Krasheninnikov, and R. M. Nieminen, J. Phys.: Condens. Matter **24**, 424218 (2012).
[55] K. Choudhary, I. Kalish, R. Beams, and F. Tavazza, Sci. Rep. **7**, 5179 (2017).
[56] M. Ashton, J. Paul, S. B. Sinnott, and R. G. Hennig, Phys. Rev. Lett. **118**, 106101 (2017).
[57] C. Kittel, *Introduction to Solid State Physics*, 7th ed. (John Wiley & Sons, New York, 1996).
[58] M. Born and K. Huang, *Dynamical Theory of Crystal Lattices (Oxford Classic Texts in the Physical Sciences)* (Clarendon Press, Oxford, 1998).
[59] F. Mouhat and F.-X. Coudert, Phys. Rev. B **90**, 224104 (2014).
[60] H. Peelaers and C. G. V. de Walle, J. Phys. Chem.C **118**, 12073 (2014).
[61] J. Feldman, J. Phys. Chem. Solids **37**, 1141 (1976).
[62] S. Lebègue, T. Björkman, M. Klintenberg, R. M. Nieminen, and O. Eriksson, Phys. Rev. X **3**, 031002 (2013).
[63] Y. Zhu, X. Kong, T. D. Rhone, and H. Guo, Phys. Rev. Mater. **2**, 081001 (2018).
[64] C. M. O. Bastos, F. P. Sabino, P. E. F. Junior, T. Campos, J. L. F. D. Silva, and G. M. Sipahi, Semicond. Sci. Technol. **31**, 105002 (2016).
[65] I. G. Lezama, A. Ubaldini, M. Longobardi, E. Giannini, C. Renner, A. B. Kuzmenko, and A. F. Morpurgo, 2D Mater. **1**, 021002 (2014).
[66] K. K. Kam and B. A. Parkinson, J. Phys. Chem. **86**, 463 (1982).